Technical Report

In-situ and Non-destructive Analysis of Protective Coatings on Structural Materials for Chemical Plants

Takashi DOI*

Abstract

To improve the reliability of structural materials for energy production exposed to harsh corrosive environments, the protective properties of the films formed at the interface between the environment and the material are important. To understand the formation and degradation mechanisms of protective films, it is desirable to extract as much information as possible about these films in the functional state. Non-destructive and in-situ analysis methods were studied for this purpose. As a result of applying these methods, the mechanism of gas reaction inhibition by Cu addition to metal dusting corrosion in the GTL fuel fabrication process and the mechanism of corrosion inhibition by Cr in low-alloy Oil Country Tubular Goods materials in a CO_2 environment were elucidated.

1. Introduction

Steel manufacturers are actively engaged in the research and development of structural materials for chemical plants that not only provide a stable supply of energy, but also produce new energy, aiming to reduce carbon dioxide (CO_2) emissions. These materials are used in energy production and support our living infrastructure and are often exposed to harsh environments such as high temperatures and high pressures. Oxide films are formed on the surfaces of materials exposed to such environments due to their interaction with the environment. The durability and reliability of materials depend on the characteristics of this oxide film. The composition and structure of the interface containing the oxide film contain information that reflects the oxidation resistance and reactivity of the material in its operating environment. During evaluation and analysis, a lot of information must be carefully extracted.

The analysis uses a method whereby "probe" particles are irradiated and impinged onto the target substance, and the various particles emitted as a result of various interactions within the substance are detected as information. The range of information to be obtained is wide, such as the amount, existence state, crystal structure, etc., and the examination method is flexible. It is necessary to use appropriate methods depending on the target substance and the information required. We are proceeding with the study and development of analysis techniques to elucidate the protectivity of films and their deterioration mechanisms. New corrosion resistance and oxidation resistant mechanisms obtained from analysis of the protectivity and deterioration behavior of films formed on surfaces are implemented for research on the reliability improvement of structural materials.

The recent energy situation has led to an increase in the severity of the environment where structural materials for energy production plants are used. As a result, examples have been observed where oxidation and deterioration behavior proceed through processes different from those previously known. Unconventional approaches and analysis methods are needed to analyze the oxidation and deterioration proceeding at the interface between the operating environment and materials and the factors that suppress and control them. Attention is focused on nondestructive analysis and in-situ analysis methods to analyze the surface films formed in such harsh environments, clarify their surface reactions, and extract the maximum amount of information. In Chapter 2, we introduce the nondestructive analysis[1] of the scale/base metal interface using hard X-ray photoemission spectroscopy (HAXPES). Chapter 3 introduces a high-temperature and high-pressure moisture optical analysis cell and describes the in-situ analysis[2] of corrosion product films using the optical cell and Raman scattering spectroscopy.

2. Nondestructive Analysis of Scale/Base Metal Interface by HAXPES

Recently, GTL (gas to liquids)[3] and DME (dimethyl ether),[4] clean fuels made from natural gas, have been attracting attention as

* Ph.D., Senior Researcher, Materials Microstructure Characterization Research Dept., Materials Characterization Research Lab., Advanced Technology Research Laboratories
1-8 Fuso-Cho, Amagasaki City, Hyogo Pref. 660-0891

new sources of energy that are advantageous in reducing CO_2 emissions. Recently, it has been pointed out that severe corrosion called metal dusting (MD) corrosion[5] may occur in the GTL and DME manufacturing processes.[6] The MD corrosion behavior differs depending on the alloy composition. For example, in low-alloy steel, whose main component is Fe, CO in these synthesis gases is adsorbed on the steel surface and carburizes it, and Fe_3C is formed near the steel surface. On the Fe_3C surface, carbon is deposited by the reaction with the synthesis gas (syngas), Fe_3C is re-decomposed into Fe and graphite, and fine Fe particles fall off. After Fe flakes off, Fe_3C is formed again at the interface between the steel and the syngas. The repeated generation and decomposition of Fe_3C causes significant corrosion thinning.[7] On the other hand, stainless steel and Ni-based alloys exhibit different corrosion behavior. A protective film is formed on the surfaces of these metals, even in a syngas environment. Still, carburization of the base metal progresses through exposed metal regions, such as film cracks and peel-off that inevitably occur during use. As carburization proceeds, compounds like $M_{23}C_6$ and M_7C_3 are formed with Cr as the main component, and graphite also precipitates on the surface of the base metal. It is thought that as a result, the metal flakes off and pit corrosion progresses.[8–10]

Conventional materials are not suitable for long-term use in corrosive environments, making it challenging to design equipment for producing syngas like GTL. To address this issue, Nippon Steel Corporation conducted internal studies and discovered that Ni-based alloys containing Cr, Cu, and Si are less susceptible to corrosion in such environments.[11] As a result of this research, NEXAGE™696 (Ni-30Cr-2Cu-1.5Si)[12] was developed based on a new corrosion protection concept as a result of mechanism elucidation research. The study found that Cr and Si in the developed material form a protective oxide layer in an MD environment, but the effect of Cu was not very clear. To clarify this point, a study was conducted using Ni, Cu, and various Ni-Cu binary alloys.[11] The study found that Cu is less likely to cause MD corrosion and is considered to be low in the adsorption activity of CO, which is the main cause of MD corrosion. Although Ni is subject to MD corrosion, MD corrosion was largely suppressed in the Ni-Cu alloys. It is well known that Cu segregates on the surface of Ni-Cu alloys at high temperatures.[13] Even for Ni-Cu alloys that exhibited MD corrosion resistance, heating experiments in an ultra-high vacuum confirmed that Cu segregated on the surface. In other words, in the developed material as well, there was a high possibility that Cu would segregate on the base metal surface directly below the protective scale in the high-temperature syngas environment. When defects are inevitably formed in the protective scale in the operating environment, Cu migrates to the surface defects in the base metal and suppresses the dissociative adsorption of CO and, hence, the MD corrosion resistance of the developed material can be well understood. To verify this idea, it is crucial to obtain detailed information on the composition and chemical bonding state in the depth direction of test specimens exposed to a simulated syngas environment. After evaluating various methods, we discovered that the distribution and existence state of Cu and other alloying elements at the scale/base metal interface could be analyzed by nondestructive in-depth analysis with the HAXPES method. This method excites photoelectrons with large kinetic energy by using hard X-rays as a radiation source. Unlike normal XPS, XPS measurements using hard X-rays can acquire XPS spectra at several tens of nanometers or more than 10 times the information depth of normal XPS. When we perform angle-resolved

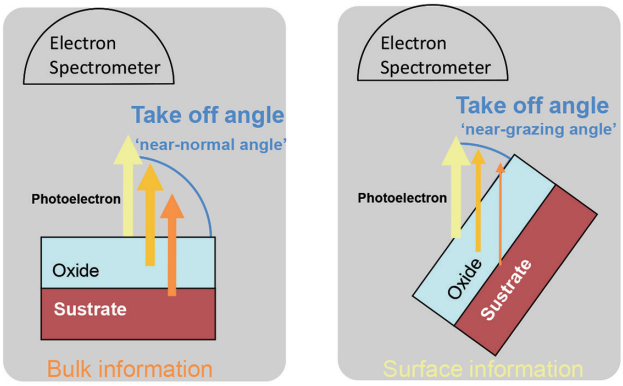

Fig. 1 Schematic diagram of angle resolved XPS

measurements using this HAXPES and with the specimen tilted relative to the photoelectron analyzer, as shown in **Fig. 1**, we can obtain information on the depth distribution and existence state of each element, including Cu.

Two types of specimens were prepared: alloy 1 and alloy 2. Alloy 1 has MD corrosion resistance in a syngas environment, but alloy 2 promotes MD corrosion. The composition is Ni-22Cr-2Cu for alloy 1 and Ni-22Cr-1Cu for alloy 2. The two alloys were subjected to an oxidation test at 650°C for 600 s in a simulated syngas environment (60%CO + 26%H_2 + 11.5%CO_2 + 2.5%H_2O) and then immediately taken out and used for measurements.

HAXPES measurements were conducted at SPring-8 BL47XU using 8 KeV X-rays. The measurements were performed using the angular resolution method, and the photoelectron take-off angle (TOA) was set to 80, 52, 30, and 15 deg.

Figure 2 shows representative spectra obtained from alloy 1. The Cr 2p3/2 peak shown in Fig. 2(a) consists of the low binding energy component (Met. Cr) that has spectral information from a metal component and the low binding energy component (Cr-O) that has spectral information from an oxide (Cr-O). The Ni 2p3/2 spectrum shown in Fig. 2(b) and the Cu 2p3/2 spectrum shown in Fig. 2(c) suggested that both Ni and Cu exist mainly in the metallic state, respectively. Although not shown here, O 1s and C 1s spectra were also obtained. Among these, C 1s had two components: hydrocarbon (CH) and graphite (C).

All photoelectron peaks were background processed by the Shirley method.[14] Cr 2p3/2 and C 1s were fit by the Voigt function and separated into the respective components. **Figure 3** shows the element concentrations obtained from these integrated peaks using the theoretically calculated photoionization cross sections of Yeh et al.[15] The TOA dependence of the concentration of each element constituting alloy 1 and alloy 2 can be roughly divided into three groups. First, the concentration ratios of Ni, Cu, and Cr-Met. tended to decrease as the TOA became shallower. C and CH showed the opposite trend, with the concentration ratio increasing as the TOA became shallower. Cr-Ox and O exhibited maximum values near a TOA of 30 deg. These behaviors for TOA reflect a characteristic distribution in the depth direction. For example, the behavior that the concentration ratio of C and CH components increases as the TOA becomes shallower indicates that they are distributed toward the surface. On the other hand, Cr-Met., Ni, and Cu, which showed the opposite tendency, are distributed on the lower layer side. Due to their TOA dependence, Cr-Ox and O components are distributed between the C and CH groups and the Cr-Met., Ni, and Cu groups. These Cr-Ox and O components constitute a protective scale, and

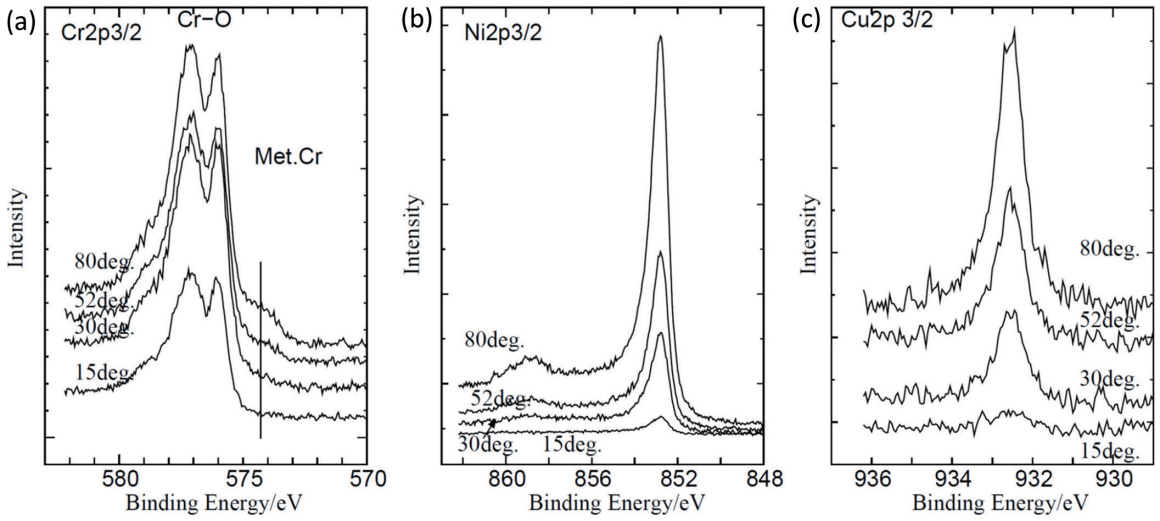

Fig. 2 Angle-resolved XPS spectra of each element in alloy1[1)]
(a) Cr 2p3/2 spectrum. In the figure, Met.Cr indicates the metallic component and Cr-O the oxide component. (b) Ni 2p3/2 spectrum. (c) Cu 2p3/2 spectrum.

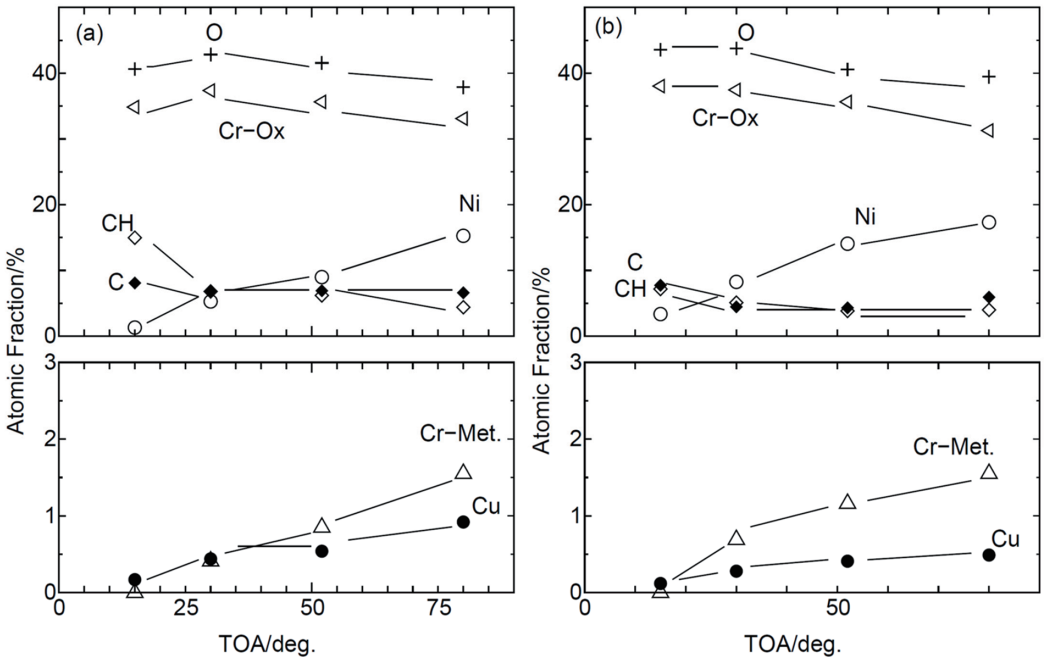

Fig. 3 Angular dependence of the quantitative values of each element on the take-off angle of photoelectron[1)]
(a) alloy1, (b) alloy2. In the figure, Cr-Met. is the Cr metal component, Cr-Ox is Cr the oxide component, and CH is the hydrocarbon component.

Cr-Met., Ni, and Cu correspond to the base metal components directly below the scale. C and CH were distributed on the outermost surface of the specimen, which was closest to the environment. From this C distribution and photoelectron peak profile, it is thought that graphite was formed on the outermost surface due to the progress of CO decomposition in the environment. Regarding the CH component, it cannot be determined whether it is derived from reaction products in the simulated syngas or from surface contamination after specimen removal.

What needs to be clarified is the existence state of Cu and its depth distribution. Cu existed in a metallic state. From its angular resolution behavior, Cu is judged to be a base metal component just below the scale, along with Cr-Met. and Ni. To confirm the depth distribution of the three components Cr-Met., Ni, and Cu, the concentration ratio with respect to the TOA was calculated using only the three components. The results are shown in **Fig. 4**. The Cr-Met. component ratio decreased as the TOA decreased. On the other hand, the Ni and Cu component ratios increased as the TOA decreased. These TOA profiles show that Ni and Cu were distributed relatively more on the surface side than Cr-Met. Since Cr is consumed as an oxide, it tends to be depleted at the interface between the scale and the base metal. The angle-resolved measurement re-

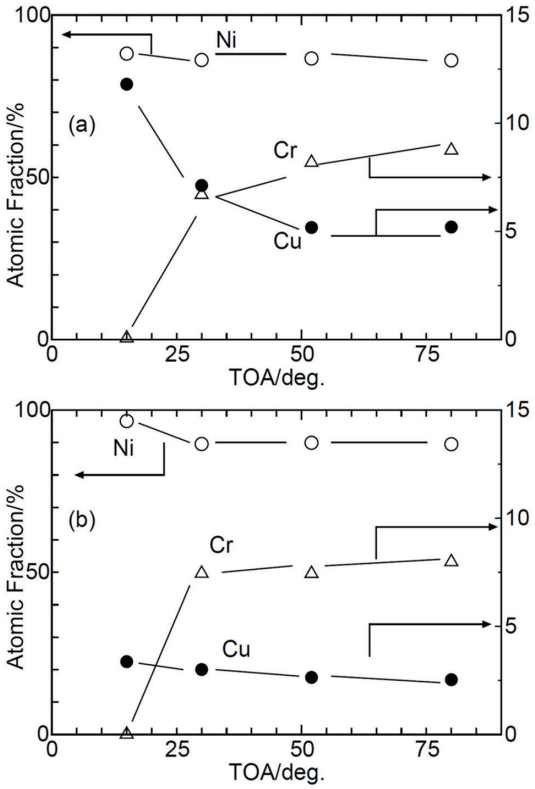

Fig. 4 Dependence of Cr metallic component, Cu, and Ni components on the take-off angle of photoelectron[1)]
(a) alloy1, (b) alloy2.

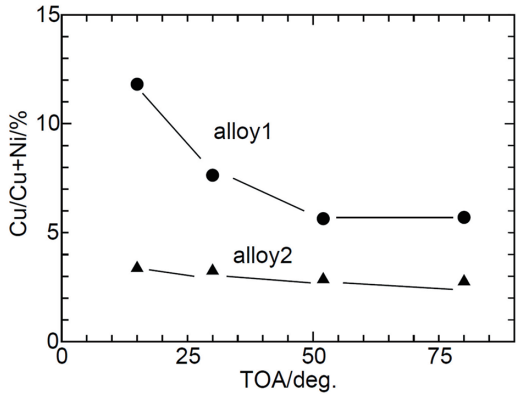

Fig. 5 Dependence of Cu and Ni ratio on the take-off angle of photoelectron[1)]

sults with HAXPES are thought to reflect this tendency. Furthermore, to clarify the difference in the in-depth distribution of Ni and Cu, **Fig. 5** shows the concentration ratio of Cu and Ni. It was shown that in both alloys 1 and 2, Cu tends to exist more on the surface side than Ni. This means that immediately below the scale and base metal interface, Cu is more abundant than the bulk composition; that is, it tends to segregate on the surface. As is clear from Fig. 5, the Cu concentration at this interface is higher in alloy 1, which suppresses the MD corrosion, than in alloy 2. By adding further analysis to the measurement results obtained using the angle-resolved HAXPES method, quantitative information on the composition and thickness of each component can be obtained.[1)] As a result, the Cu concentration at the interface was more than twice as high in alloy 1 than in alloy 2. This difference in the Cu concentration at the interface is thought to have greatly contributed to the suppression of the progress of carburization through protective scale defects and determined the difference in MD corrosion resistance.

As mentioned at the beginning, surfaces and interfaces contain information that reflects the oxidation resistance, reactivity, etc., of materials in their operating environment. It is necessary to extract this information carefully. Destructive analysis is often applied by using Ar^+ sputtering, but this causes considerable damage to the surface and interface of the specimen. Nondestructive extraction of information often leads to the elucidation of essential phenomena.

3. In-situ Analysis of Effect of Cr Action on Corrosion Resistance Improvement of Oil Country Tubular Goods (OCTGs) in CO_2 Corrosion Environment

Oil and natural gas are still important energy sources that support our daily lives, and their stable supply is required from the perspective of energy security. Recently, drilling from deeper locations has become necessary, and the development of deep, highly corrosive wells has been increasing. As a result, OCTG materials are required to have higher strength and corrosion resistance than ever before. Corrosive environments are high-temperature and high-pressure water environments with temperatures ranging from several tens of degrees Celsius to over 300°C. These environments contain many corrosive gases such as H_2S and CO_2, but the concentration of O_2, which is essential for the formation of a protective oxide film, is low. These environments are very severe for structural materials. Nippon Steel has continued to promote the development of corrosion-resistant materials that can be used in these harsh environments. Most corrosion tests are conducted in a sealed pressure-resistant vessel called an autoclave, which can simulate a high-temperature and high-pressure environment. Specimens may deteriorate as they are moved from a high-temperature and high-pressure water environment, which is a corrosion environment, through a normal-temperature and normal-pressure environment into an evaluation and analysis unit. This makes it difficult to have a detailed discussion on the corrosion mechanism. Therefore, we proceeded with the development of a high-temperature and high-pressure spectroscopy cell that can simulate a severe high-temperature and high-pressure corrosive environment and can also conduct the in-situ analysis of surface films, which are key to the corrosion resistance of steel. As part of this activity, we present the results of a study on the corrosion resistance of OCTGs in a CO_2 corrosion environment.

It is widely known that the addition of Cr is effective in improving the corrosion resistance of OCTGs in a CO_2 corrosion environment.[16)] Cr-containing steel exhibits characteristic corrosion behavior in this environment. For example, the peak corrosion rate decreases as the amount of Cr added increases but shifts to the high end of the temperature range.[17, 18)] On the other hand, the reason is not clear. Also, the effectiveness of $FeCO_3$ as a protective film for low-alloy steel is well known.[19)] It is also well known that films on steel containing 9% or more of Cr also have films that are high in Cr content and low in crystallinity.[20)] There are surprisingly few examples of detailed research into the action of Cr and its effect on corrosion resistance, as compared to the importance of the material and its operational history since development. The reason for this is presumably because many things were not clarified by the evaluation

and analysis of specimens removed from the high-temperature and high-pressure autoclave at room temperature. We investigated this action of Cr using the developed spectroscopy cell.

This spectroscopy cell is made of a Ni-based alloy that has corrosion resistance in H_2S-containing OCTG operating environments. To allow spectroscopic analysis with the use of an optical microscope, the spectroscopy cell is designed by considering the objective lens working distance and can be used together with a commercial micro-Raman scattering spectrometer.[21)]

The specimen materials were Fe-0.01C-xCr alloy (x = 0, 1, 2, 3, 5, 9, 13) and the specimen surfaces were mirror-polished. A 5 wt% NaCl solution was prepared. The specimen was installed in the cell, and the atmosphere in the cell and piping was replaced with CO_2 gas. The test solution was introduced into the liquid bottle, and the cell was pressurized and degassed with the CO_2 gas. A liquid pump sent the test solution into the cell at 0.5 ml/60 s. A heater was installed in the cell and used to adjust the cell to the test temperature quickly. The internal pressure of the cell was adjusted with a back pressure valve located downstream so that it was always 3.0 MPa. During the test, a pump constantly supplied the test solution, and the solution that came into contact with the specimen was directly discharged outside. The discharged solution was used for analysis by ICP-AES (Inductively Coupled Plasma Atomic Emission Spectroscopy) as required. Immediately after the solution was introduced, microscopic observation and micro-Raman scattering spectroscopy analysis were performed during the heating process. An LD laser (532.05 nm) was used for Raman scattering spectroscopy, and spectra were obtained with a diffraction grating spectrograph. The cell temperature was maintained at 100°C, 150°C, or 200°C. The specimens were maintained at each temperature for 3 600 s and were observed and analyzed.

Figure 6 shows changes in the appearance of 0Cr, 2Cr, and 5Cr specimens by fixed point observation immediately after heating to 200°C (early stage), at about 600 s later (middle stage), and at about 1 800 s later (later stage). The observed corrosion process is supplemented below. For the 0Cr and 1Cr specimens, corrosion products were observed to flow through the solution from a relatively low temperature of 100°C or less during the heating process. This suggests that the 0Cr and 1Cr specimens were severely corroded. On the other hand, for the 2Cr and 5Cr specimens, no corrosion products were observed to flow in the solution. This suggests that Cr acts as a corrosion inhibitor from the early stage of corrosion.

For the 0Cr specimen, corrosion products were observed to flow in the solution for a while after reaching the predetermined test temperature. When the granular corrosion products indicated by the red circles in Fig. 6 started to be observed on the 0Cr specimen surface, the corrosion products flowing in the solution gradually began to decrease. The granular products formed on the specimen surface grew with the holding time. In the later stage, when the 0Cr specimen was held at 200°C, corrosion products were no longer observed to flow in the test solution. This suggested that the granular corrosion products acted protectively. Furthermore, these granular corrosion products tended to form and grow more quickly as the test temperature increased. The granular corrosion products behaved in the 1Cr specimen in almost the same way as in the 0Cr specimen.

Figure 6 shows the changes in the appearance of the 2Cr specimen during the heating process. Unlike the 0Cr and 1Cr specimens, the base metal surface of the 2Cr specimen exhibited hues that appeared like interference colors. The interference colors showed different tones for different base metal grains and changed moment by moment as the corrosion progressed. This color tone change was observed in all specimens containing 2% or more Cr. We thought that an extremely thin corrosion product film had probably formed and gradually changed in thickness. In addition, the degree of this color tone change differed with the Cr content. In the case of the 2Cr specimen, the corrosion product film grew thickly in the later stage at about 1 800 s after reaching 200°C. Consequently, few bright interference colors were seen. The grains appeared black or

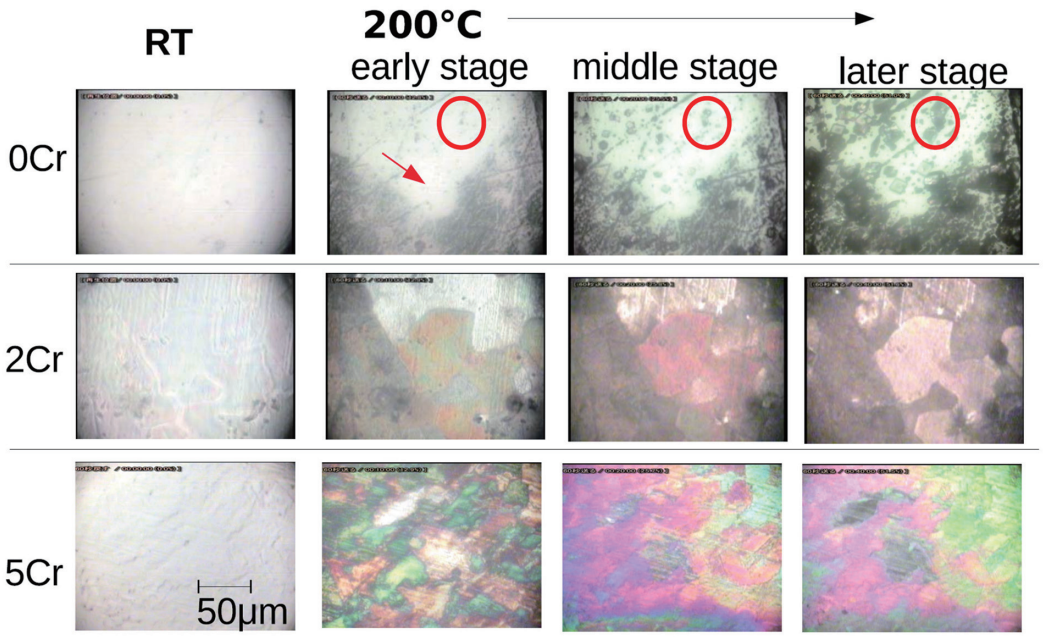

Fig. 6 The results for 0Cr, 2Cr, and 5Cr specimens at room temperature, immediately after heating up to 200°C (early stage), about 600 s after reaching 200°C (middle stage), and about 1 800 s (later stage). The red circles in the figure indicate corrosion products of interest.[2)]

gray on the whole, although they individually differed in brightness and darkness. Specimens containing 3% or more Cr showed bright interference colors from the early stage, like the 2Cr specimen. Steel specimens containing 3% or more Cr were held in such a condition that the interference colors could be confirmed up to 3 600 s after the observation was completed, although the color tone changed. Figure 6 shows a representative change in the appearance of the 5Cr specimen. Although it cannot be clearly identified in the micrographs of Fig. 6, granular corrosion products similar to those of the 0Cr and 1Cr specimens were observed in the 2Cr specimen after the middle stage and in the 3Cr specimen in the later stage.

Raman spectra were obtained from the respective regions of the specimens while observing the images. Representative spectra are shown in **Figs. 7** to **10**.

The spectra shown in Fig. 7 were obtained from the 0Cr specimen, regardless of the experimental temperature. A spectrum showing no clear peak and indicated as position 1 was obtained over a wide range. A spectrum with a sharp Raman peak indicated as position 2 was obtained from the granular corrosion products indicated by the red circles in the microphotographs of the 0Cr specimen in Fig. 6. The position 2 spectrum matched well with the Raman spectrum of $FeCO_3$.[22] A similar spectrum was detected from the granular corrosion products of the 1Cr specimen. In these specimens, $FeCO_3$ was formed in the early stage and was detected from almost the entire surface from the later stage to the end of the experiment, regardless of the temperature.

For specimens containing more than 2% Cr, spectra different from those of the 0Cr and 1Cr specimens were collected, as shown in Fig. 8. The spectrum acquired in the early stage was obtained from the region exhibiting the interference colors confirmed in Fig. 6. This spectrum has characteristics of spinel-type iron oxide.[23] In the 2Cr specimen, $FeCO_3$ also began to be confirmed from the middle stage onwards. Although there was a tendency for $FeCO_3$ to increase over time, during the observation period, it did not cover the entire surface, unlike the 0Cr and 1Cr specimens.

Figure 9 shows the Raman spectra obtained from the 3Cr specimen. In the early stage, a Raman spectrum with a peak around 520 cm^{-1} was observed. After that, a spectrum with peaks around 670 cm^{-1} and 550 cm^{-1} began to be observed, and the spectrum with a peak around 520 cm^{-1} was no longer observed. This spectrum change over time was similar to that for the 5Cr specimen. Among these spectra, the corrosion products with peaks near 670 cm^{-1} and 550 cm^{-1} match the characteristics of spinel-type iron oxide, which was also confirmed in the 2Cr specimen. On the other hand, we believe that the spectra observed in the 3Cr and 5Cr specimens, mainly in the early stage, are highly likely to be spectra from $Cr(OH)_3$. Al-

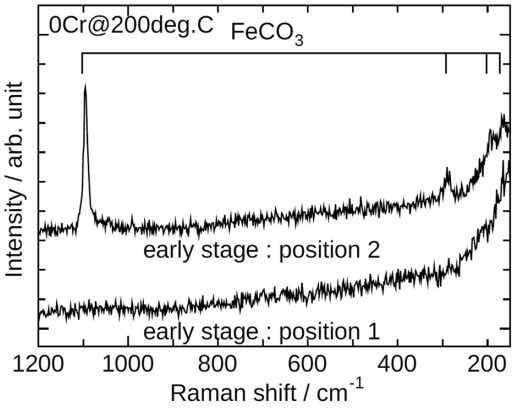

Fig. 7 Raman spectra from 0Cr at 200°C, early stage[2]

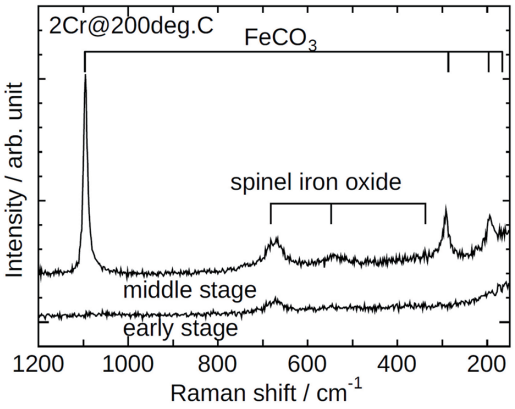

Fig. 8 Raman spectra from 2Cr material at 200°C[2]
Spectra observed at the early stage and middle stage are shown, respectively.

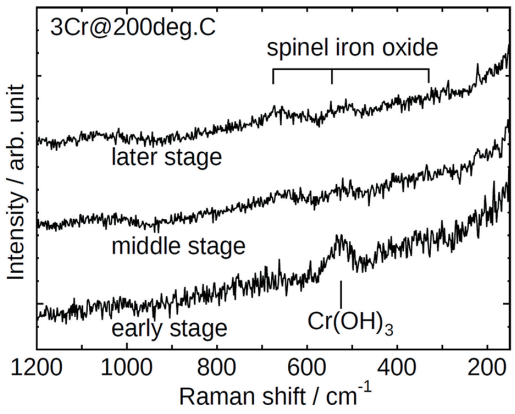

Fig. 9 Raman spectra from 3Cr material at 200°C[2]
Spectra observed at the early stage, middle stage, and later stage are shown, respectively.

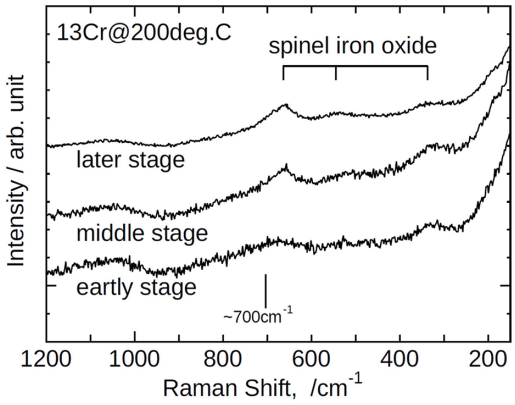

Fig. 10 Raman spectra from 13Cr material at 200°C[2]
Spectra observed at the early stage, middle stage, and later stage are shown, respectively.

though there are not many reports on the spectra of oxides with a peak around 520 cm^{-1}, Melendres et al.[24] reported the presence of $Cr(OH)_3$ exhibiting a broad peak near 520 cm^{-1} on the surface of Cr containing steel in a high-temperature and high-pressure water environment. Brook et al.[25] also pointed out that the stability range of $Cr(OH)_3$ expands under high-temperature water.

This $Cr(OH)_3$ was observed only in the early stage immediately after the temperature rise when the specimen was maintained at 200°C. Still, it tended to be observed even after the early stage when the specimen was maintained at 100°C and 150°C. This is probably due to the fact that heating to 200°C takes time compared to heating to 100°C or 150°C. In other words, we believe that spinel-type iron oxide was subsequently deposited on the $Cr(OH)_3$ formed during the heating process to 200°C, making it difficult to observe $Cr(OH)_3$.

Figure 10 shows Raman spectra obtained from the 13Cr specimen at 200°C. Only a Raman spectrum with characteristics of spinel-type iron oxide was observed from the early stage immediately after heating up until the end of the observation. However, the Raman spectrum is characterized by a shoulder peak around 700 cm^{-1} with a tail at the high end of the frequency range as compared to the spectrum of spinel iron oxide observed in the 2Cr specimen shown in Fig. 8. For example, the Raman spectrum of $FeCr_2O_4$[26] is well known as a Raman spectrum exhibiting such characteristics. A spectrum of spinel iron oxide with similar characteristics was also observed on the surface of the 9Cr specimen. It is highly likely that the spinel iron oxide formed on the surface of high Cr content steels, such as the 9Cr and 13Cr specimens, contains spinel-type complex iron with a high Cr content, such as $FeCr_2O_4$.

The formation behavior of corrosion products on the surface of a Fe-Cr alloy was tracked using micro-Raman scattering spectroscopy in a high-temperature and high-pressure CO_2 gas-containing aqueous solution environment. **Table 1** summarizes the changes over time in the corrosion products formed on Cr-containing steels in the CO_2 corrosion environment where OCTGs are used. Up until now, it has been difficult to observe and discuss corrosion products as they change over time depending on the composition of the steel and the corrosive environment. In-situ analysis has confirmed this change over time for the first time.

In this environment, the results of solution analysis by ICP-AES conducted at the same time as the observation and the results of XPS analysis of the specimens removed from the cell were added to the changes in the corrosion products with the Cr content, temperature, and time revealed by the in-situ analysis. **Figure 11** summarizes the Cr action in the environment discussed above. For details, refer to Reference 2). The results are outlined below.

When the specimen contains less than about 2% Cr, $FeCO_3$ begins to precipitate from the early stage of corrosion, as shown in **Fig. 12**. However, the $FeCO_3$ crystals start to become granular, spread in the in-plane direction, and cover the surface at least after the later stage. The corrosion is thought to continue to some extent until then.

On the other hand, in the case of Cr-containing steel (Fig. 11), during the initial stage of corrosion, base metal components such as Fe and Cr are severely corroded and eluted in an aggressive CO_2 corrosion environment.[27] However, the eluted Cr quickly forms corrosion products with low solubility and begins to precipitate directly on the base metal as $Cr(OH)_3$. Fe^{2+} eluted at the same time also begins to form Fe oxide. The formation of $FeCO_3$ was suppressed by the action of Cr^{3+} ions coexisting in the solution. In most cases, a thin and relatively uniform film was quickly formed as spinel-type iron oxide, suppressing its elution from the base metal.

Changes over time in the process leading to material deterioration or the acquisition of protective properties can be investigated not only by in-situ analysis of corrosion products, but also by using experimental data such as surface morphology, color, texture, and the amount of corrosion and elution during that time. By combining this information with previous knowledge, we were able to under-

Table 1 Changes over time of corrosion products revealed by in-situ analysis[2]

Specimen	Temperature(°C)	Elapsed time after temperture increase		
		Early stage	Middle stage	Later stage
0Cr	100	$FeCO_3$	→	→
	150	$FeCO_3$	→	→
	200	$FeCO_3$	→	→
1Cr	100	$FeCO_3$	→	→
	150	$FeCO_3$	→	→
	200	$FeCO_3$	→	→
2Cr	100	SP	SP+$FeCO_3$	→
	150	SP	SP+$FeCO_3$	→
	200	SP	SP+$FeCO_3$	→
3Cr	100	$Cr(OH)_3$	SP	SP+$FeCO_3$
	150	$Cr(OH)_3$	SP	SP+$FeCO_3$
	200	$Cr(OH)_3$+SP	SP	SP+$FeCO_3$
5Cr	100	$Cr(OH)_3$	SP	SP+$FeCO_3$
	150	$Cr(OH)_3$	SP	SP+$FeCO_3$
	200	$Cr(OH)_3$+SP	SP	SP+$FeCO_3$
9Cr	200	SP	→	SP+$FeCO_3$
13Cr	200	SP	→	→

SP: Spinel iron oxide

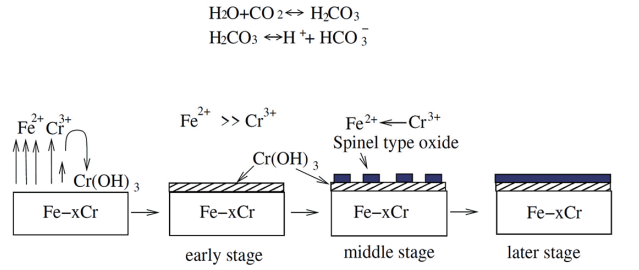

Fig. 11 Schematic diagram of time-dependent corrosion products changing on chromium-containing steels with chromium at a 2 mass% or higher content[2]

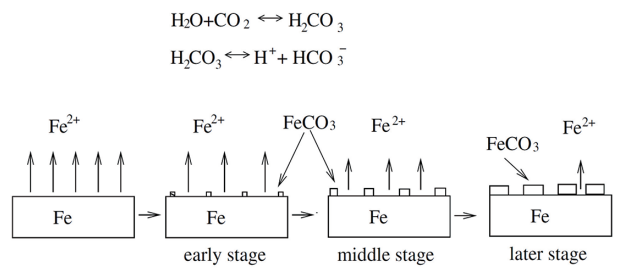

Fig. 12 Schematic diagram of time-dependent corrosion products changing on steels with less than 2 mass% chromium[2]

stand the phenomena occurring on the material surface comprehensively. This method will become a useful technology for corrosion analysis of structural materials for energy production, which will be used in increasingly harsh environments.

4. Conclusions

Structural materials for energy production are exposed to harsh operating environments. Interaction with the environment forms oxide films on these materials. Information on the oxidation resistance, reactivity, etc., of materials in their operating environment is concentrated in the composition and structure of interfaces containing oxide films, which affect the durability and reliability of materials. We have introduced some nondestructive and in-situ analysis techniques that can be used to carefully extract such information and lead to understanding the phenomena involved.

As a result of the analyses, a deeper understanding of phenomena and updated material knowledge will enable the development of the next highly durable and highly reliable materials. Alloying elements play a major role in the surface functions of steel. In the cases introduced in this report, for example, Cu and Cr interacted with the local operating environment, changed their distribution, and uniquely changed their state of existence. Consequently, these elements, in turn, contributed to improvement in the surface functionality and reliability of materials. There are many cases where other alloying elements function effectively as the combination of the environment and composition varies. In the future, the steelmaking process will greatly change due to global warming countermeasures. Geopolitical risks are also expected to restrict the alloying elements that can be used. We will build elementary technologies to contribute to the development of various materials while identifying the phenomena proceeding on the surfaces of materials in severe operating environments and constantly being aware of material design techniques that make the most of the functions of these alloying elements and of how to incorporate them into the creation of the material surfaces.

References

1) Doi, T. et al.: Surf. Interface Anal. 40, 1374 (2008)
2) Doi, T. et al.: Corrosion Science. 177, 108931 (2020)
3) Tsukazaki, Y.: J. Soc. Automob. Eng. Jpn. 55 (7), 67 (2001)
4) Jpn DME Forum: DME Handbook. Jpn., Ohmsha, 2006
5) Grabk, H.J.: Carburization, A High-Temperature Corrosion Phenomenon. St. Louis, Materials Technology Institute of the Chemical Process Industries, Inc. 1998, no. 52
6) Holland, M.L. et al.: Int J. Pres. Ves. & Piping. 66, 125 (1996)
7) Grabke, H.J. et al.: Werkst. Korros. 44, 89 (1993)
8) Pipple, E. et al.: Mater. Corros. 50, 309 (1998)
9) Chun, C.M. et al.: Mater. Corros. 50, 634 (1999)
10) Nishiyama, Y. et al.: Mater. Trans. 46 (8), 1890 (2005)
11) Nishiyama, Y. et al.: Matter. Corros. 56 (11), 806 (2005)
12) Nishiyama, Y. et al.: Materia Japan. 52 (1), 23 (2013)
13) For example, Webber, P.R. et al.: Surface Science. 105, 20 (1981)
14) Shirley, D.A. et al.: Phys. Rev. B. 5, 4709 (1972)
15) Yeh, J.J. et al.: At. Data Nucl. Data Tables. 32, 1 (1985)
16) Ikeda, A. et al.: CO_2 Corrosion Behavior of Cr-containing Steels. EFC Publications, Nunber 13, 1994, p. 59
17) Ikeda, A. et al.: Corrosion/84, Paper No.289 (1984)
18) Ikeda, A. et al.: CO_2 Corrosion Behavior of Cr-Containing Steels EFC Publications no.13, 1994
19) Heuer, J.K. et al.: Corros. Sci. 41 (7), 1231 (1999)
20) Ueda, M. et al.: Corrosion/96, Paper No.13 (1996)
21) Doi, T. et al.: Corrosion Engineering. 60, 369 (2011)
22) Rull, F. et al.: J. Raman Spectrosc. 34, 267 (2003)
23) Yamanaka, K. et al.: Corrosion Engineering. 39, 249 (1990)
24) Melendres, C.A. et al.: Electrochim. Acta. 37, 2747 (1992)
25) Brook, P.A.: Corros. Sci. 12, 297 (1972)
26) McCarty, K.F. et al.: J. Solid State Chem. 79, 19 (1989)
27) For example, Burke, P.A.: Advances in CO_2 Corrosion. Vol.1, NACE 1984, p. 3

Takashi DOI
Ph.D., Senior Researcher
Materials Microstructure Characterization Research Dept.
Materials Characterization Research Lab.
Advanced Technology Research Laboratories
1-8 Fuso-Cho, Amagasaki City, Hyogo Pref. 660-0891